1 **Supporting Information**

2 **Role of Hydroxyl Radicals and Mechanism of Escherichia Coli Inactivation on**

3 **Ag/AgBr/TiO_2 Nanotube Array Electrode under Visible Light Irradiation**

4 Yang Hou,[†] Xinyong Li,[*,†,‡] Qidong Zhao,[†] Guohua Chen,[*,‡] and Colin L. Raston[§]

5 [†]*Key Laboratory of Industrial Ecology and Environmental Engineering (MOE) and State Key*

6 *Laboratory of Fine Chemical, School of Environmental Science and Technology, Dalian*

7 *University of Technology, Dalian, 116024, China*

8 [‡]*Department of Chemical and Biomolecular Engineering, the Hong Kong University of*

9 *Science & Technology, Clear Water Bay, Kowloon, Hong Kong*

10 [§]*Centre for Strategic Nano-Fabrication, School of Biomedical, Biomolecular and Chemical*

11 *Sciences, University of Western Australia, 35 Stirling Highway, Crawley, Western Australia*

12 *6009, Australia*

13 Summary: This document contains 42 pages, including 21 figures, 1 table and 1 scheme

[*] Corresponding Author. Phone: +86-411-8470-7733 (X.Y.L.); +852-2358-7138 (G.H.C.). Fax: +86-411-8470-7733 (X.Y.L.); +852-2358-0054 (G.H.C.). E-mail: xyli@dlut.edu.cn (X.Y.L.); kechengh@ust.hk (G.H.C.).

Figure Captions:

Figure S1. XRD patterns of the Ag/AgBr/TiO_2-NA.

Figure S2. (a) Ag 3d XPS spectrum of the Ag/AgBr/TiO_2-NA. (b-c) TEM images of TiO_2-NA and Ag/AgBr/TiO_2-NA. (d-e) HRTEM images of TiO_2-NA and Ag/AgBr/TiO_2-NA.

Figure S3. PL spectra of TiO_2-NA, Ag/TiO_2-NA and Ag/AgBr/TiO_2-NA.

Figure S4. UV-Vis diffuse reflectance spectra of TiO_2-NA, Ag/TiO_2-NA and Ag/AgBr/TiO_2-NA.

Figure S5. Short-circuit photocurrent time dependence of TiO_2-NA, Ag/TiO_2-NA and Ag/AgBr/TiO_2-NA under visible light irradiation ($\lambda > 420$ nm, I_0 = 25.3 mW cm^{-2}, 0.6 V vs. SCE).

Figure S6. Images of E. coli colonies on an agar plate before and after PEC inactivation treatment with Ag/AgBr/TiO_2-NA electrode for 20, 40, 60 and 80 min ($\lambda > 420$ nm, I_0 = 25.3 mW cm^{-2}, 0.6 V vs. SCE).

Figure S7. Photographs of E. coli untreated and after PEC inactivation treatment with Ag/AgBr/TiO_2-NA electrode for 80 min ($\lambda > 420$ nm, I_0 = 25.3 mW cm^{-2}, 0.6 V vs. SCE).

Figure S8. E. coli PEC inactivation efficiencies of four repeated experiments with the Ag/AgBr/TiO_2-NA electrode ($\lambda > 420$ nm, I_0 = 25.3 mW cm^{-2}, 0.6 V vs. SCE).

Figure S9. Images of E. coli colonies on an agar plate during four repeated PEC inactivation experiments with Ag/AgBr/TiO_2-NA electrode.

Figure S10. TOC removal during PEC inactivation of E. coli process with Ag/AgBr/TiO_2-NA electrode under visible light irradiation. Inset: E. coli and TOC removal during the course of

the PEC inactivation (λ>420 nm, I_0 = 25.3 mW cm^{-2}, 0.6 V vs. SCE).

Figure S11. Concentration of oxamic and oxalic acids changes with irradiation time during the PEC inactivation of E. coli by Ag/AgBr/TiO_2-NA electrode (λ>420 nm, I_0 = 25.3 mW cm^{-2}, 0.6 V vs. SCE).

Figure S12. Effect of DBPs (2 mM) on PEC inactivation of E. coli as a function of time involving the Ag/AgBr/TiO_2-NA electrode under visible light irradiation (λ>420 nm, I_0 = 25.3 mW cm^{-2}, 0.6 V vs. SCE).

Figure S13. Plots of the simultaneous evolution of DBPs concentration in the presence of E, coli under visible light irradiation (λ>420 nm, I_0 = 25.3 mW cm^{-2}, 0.6 V vs. SCE).

Figure S14. PEC inactivation of E. coli as affected by different light intensity for the Ag/AgBr/TiO_2-NA electrode under visible light irradiation (λ>420 nm, 0.6 V vs. SCE).

Figure S15. Inactivation of E. coli by direct photolysis, electrochemical process, photocatalysis and photoelectrocatalysis, respectively, with the Ag/AgBr/TiO_2-NA electrode under simulated sunlight irradiation (I_0 = 46.7 mW cm^{-2}, 0.6 V vs. SCE).

Figure S16. Images of E. coli colonies on an agar plate before and after PEC inactivation treatment with Ag/AgBr/TiO_2-NA electrode under simulated sunlight irradiation (I_0 = 46.7 mW cm^{-2}, 0.6 V vs. SCE).

Figure S17. Photographs of E. coli untreated and after PEC inactivation treatment with Ag/AgBr/TiO_2-NA electrode under simulated sunlight irradiation (I_0 = 46.7 mW cm^{-2}, 0.6 V vs. SCE).

Figure S18. TEM images of E. coli (a) untreated and (b) after PEC inactivation treatment with Ag/AgBr/TiO_2-NA electrode under simulated sunlight irradiation for 17 min (I_0 = 46.7

58 mW cm^{-2}, 0.6 V vs. SCE).

59 Figure S19. Changes of FTIR spectra of E. coli during the PEC inactivation process under

60 simulated sunlight irradiation (I_0 = 46.7 mW cm^{-2}, 0.6 V vs. SCE).

61 Figure S20. Inactivation of E. coli by PEC technology with porous TiO_2, TiO_2-NA,

62 N/TiO_2-NA, Ag/AgBr/TiO_2, apatite-covered Ag/AgBr/TiO_2 and Ag/AgBr/TiO_2-NA

63 electrodes under simulated sunlight irradiation (I_0 = 46.7 mW cm^{-2}, 0.6 V vs. SCE).

64 Figure S21. PEC inactivation of E. coli as affected by different light intensity for the

65 Ag/AgBr/TiO_2-NA electrode under simulated sunlight irradiation (0.6 V vs. SCE).

66 **Scheme Captions**

67 Scheme S1. Illustrative diagrams of the photoelectron transfer in Ag/AgBr/TiO_2-NA system

68 and their effects on bactericidal reaction.

69 **Table Captions**

70 Table S1. Assignment of the FTIR bands observed in the degradation of E.coli on

71 Ag/AgBr/TiO_2-NA electrode under visible light irradiation (λ>420 nm, I_0 = 25.3 mW cm^{-2},

72 0.6 V vs. SCE).

Preparation of Ag/TiO_2-NA, N/TiO_2-NA, Porous TiO_2 (Baram), Ag/AgBr/TiO_2, Apatite-covered Ag/AgBr/TiO_2 and Ag/AgBr/TiO_2-NA Electrodes

Ag/AgBr/TiO_2-NA electrode was synthesized by a two-step approach including an electrochemical anodization technique, followed by an in situ photo-assisted deposition strategy using precursor solution containing water, cetylmethylammonium bromide and diamminesilver (I) hydroxide.

As reference, Ag/TiO_2-NA electrode was prepared by reducing the Ag^+ ions photo-catalytically using 0.21 g of $AgNO_3$ in 2.3 mL of NH_4OH (25 wt% NH_3) solution as Ag precursor and methanol solution as hole scavenger under 500 W xenon lamp irradiation. N-doped TiO_2-NA (N/TiO_2-NA) electrode was prepared by electrochemical anodization, followed by a wet immersion in 1 M $NH_3 \cdot H_2O$ solution and annealing post-treatment.[1]

As a comparison, porous TiO_2 electrode was prepared via electrochemical anodization of Ti foil in the molten sodium nitrite and sodium nitrate mixture electrolyte (50:50 molar ratios) at voltages between 0 V and 80 V according to the previous publication by Baram et al.[2]

Ag/AgBr/TiO_2 electrode was coated on a surface-treated Ti foil by a dip-coating method using Ag/AgBr/TiO_2 powders as the precursor for comparison. The Ag/AgBr/TiO_2 powders were prepared by impregnating P-25 TiO_2 (1 g) in the aqueous solution of $AgNO_3$ (0.21 g) and NH_4OH (2.3 mL, 25 wt % NH_3) containing CTAB (1.2 g). The detailed fabrication process of the Ag/AgBr/TiO_2 powders has also been presented in the previous publication by Hu et al.[3]

Apatite-covered Ag/AgBr/TiO_2 electrode was also coated on a surface-treated Ti foil by a dip-coating method using apatite-covered Ag/AgBr/TiO_2 powders as the precursor for

95 comparison. The apatite-covered Ag/AgBr/TiO_2 powders were successfully prepared by
96 impregnating P-25 TiO_2 (1 g) and hydroxyapatite (0.05 g) in the aqueous solution of $AgNO_3$
97 (0.21 g) and NH_4OH (2.3 mL, 25 wt % NH_3) containing CTAB (1.2 g). The detailed
98 fabrication process of the apatite-covered Ag/AgBr/TiO_2 powders has also been reported by
99 Elahifard et al.[4]

100 Although in our case, the mass of Ag/AgBr/TiO_2 electrode and apatite-covered
101 Ag/AgBr/TiO_2 electrode was not controlled as the same as that of Ag/AgBr/TiO_2-NA
102 electrode, the macro-areas of the three samples were similar and the illumination area was
103 constant for them. The obtained Ag/AgBr/TiO_2 electrode and apatite-covered Ag/AgBr/TiO_2
104 electrode were thick enough for full absorption of the incident visible light. Therefore, it is
105 reasonable to directly compare the PEC activity for E. coli inactivation over different
106 samples.

107 **Characterization**

108 The morphology of the Ag/AgBr/TiO_2-NA was characterized using an environmental
109 scanning electron microscope with an accelerating voltage of 30 kV (ESEM; Quanta 200
110 FEG) and transmission electron microscopy using Tecnai G2 S-Twin electron microscope
111 operated at 200 kV. The crystallinity of the prepared samples was determined from XRD
112 using a diffractometer with Cu Kα radiation (Shimadzu Lab-X XRD-6000, Source light at the
113 wavelength (λ) of 0.15406 nm). The accelerating voltage and applied current were 40 kV and
114 30 mA, respectively. Light absorption properties were measured using UV-Vis DRS (JASCO,
115 UV-550) with a wavelength range of 200-700 nm. XPS (PHI 5600 mode) was performed to
116 examine the surface properties and composition of the sample. All the binding energies were

calibrated by using the contaminant carbon (C 1s) 284.6 eV as a reference. The electron spin resonance (ESR) signals of radicals trapped by 5, 5-dimethyl-l-pyrroline N-oxide (DMPO) were detected at ambient temperature on a Bruker (E 500) spectrometer. The irradiation source was a Quanta-Ray Nd: YAG pulsed laser system (λ = 532 nm, 10 Hz). The settings for the ESR spectrometer were as follows: center field, 3443 G; sweep width, 100 G; microwave frequency, 9.64 GHz; modulation frequency, 100 kHz; power, 10.05 mW. To minimize measurement errors, the same quartz capillary tube was used throughout the ESR measurements. Total organic carbon (TOC) was measured using a Shimadzu Corporation TOC-V wp Analyzer (Japan). The concentrations of oxamic acids, oxalic acids and DBPs were determined by high performance liquid chromatography (HPLC, Waters 2695, Separations module) with a Sunfire^{TM} C18 (5 μm) reverse-phase column at 30 °C equipped with photodiode array detector (Waters 2996).

Photoelectrochemical Measurements

Photocurrent density was measured using a CHI electrochemical analyzer (CH instruments CHI 760C, Shanghai Chenhua, China) in a standard three-electrode configuration with the Ag/AgBr/TiO_2-NA electrode as photoanode (an effective area of 6 cm^2), a Pt foil as counter electrode, and a saturated calomel electrode (SCE) as reference electrode. 0.01 M Na_2SO_4 (100 mL) purged with N_2 was used as the electrolyte. A 500 W high-pressure xenon short arc lamp (Phillips) with a filter to remove light of wavelength below 420 nm was used as the visible light source to provide a light intensity of 100 mW cm^{-2}.

Antibacterial Activity Tests

E. coli was incubated in Luria Bertani nutrient solution at 37 °C for 12 h with shaking and

139 then washed by centrifuging at 4000 rpm. The treated cells were then re-suspended and
140 diluted to about 1.2×10^7 cfu mL^{-1} with 0.9% saline. The bactericidal experiments were
141 performed in a single photoelectrochemical compartment with an effective volume of 100 mL.
142 The Ag/AgBr/TiO_2-NA photoanode was in parallel with the platinum foil cathode in the
143 quartz reactor with magnetic stirring, and a SCE served as the reference electrode. All the
144 electrodes were connected to a CHI 760C electrochemical analyzer and bias potential applied
145 on the photoanode was 0.6 V (vs. SCE). A 500 W Xe lamp (Phillips, I_0 = 46.7 mW cm^{-2}), as a
146 solar simulator, was applied as the radiation source. In addition, the Xe lamp (Phillips, 500 W)
147 with a UV-cutoff filter was also used as the visible light source ($\lambda > 420$ nm), and the average
148 light intensity was 25.3 mW cm^{-2}. The system was cooled by wind and water to maintain its
149 room temperature. Prior to irradiation, the suspensions were magnetically stirred in the dark
150 for 30 min to establish adsorption-desorption equilibrium between the E. coli and the surface
151 of the photocatalyst. At regular time intervals, an aliquot of the reaction solution was
152 immediately diluted with saline and spread uniformly over nutrient agar plates, which were
153 then incubated at 37 °C for 12 h in dark before the bacterial colonies were counted. All of the
154 above experiments were repeated three times and the average values were given. All
155 materials used in the experiments were autoclaved at 121 °C for 20 min to ensure sterility.
156 The bacterial suspensions at different irradiation times were evaporated by a freeze-drying
157 method to perform the Fourier transform infrared (FTIR) spectra analysis. For FTIR
158 measurement, the dry residue was supported on KBr pellets and the FTIR spectra were
159 recorded on a VERTEX 70-FTIR spectrophotometer. At every time interval, 1 mL of the
160 bacterial suspension was centrifuged, and the supernatant was collected to determine K^+

161 leakage from the inactive bacteria by a Perkin-Elmer Analyst 700 atomic absorbance
162 spectrometer. To investigate the Ag^+ eluted from Ag/AgBr/TiO_2-NA electrode during PEC
163 inactivation of E. coli process, the Ag/AgBr/TiO_2-NA electrode/E. coli solution before and
164 after PEC treatment was respectively collected and filtered through a Millipore filter (pore
165 size of 0.45 μm). After filtration, Ag^+ concentration was measured by the Perkin-Elmer
166 Analyst 700 atomic absorbance spectrometer. All the above experiments were also conducted
167 in triplicates.

168 **Analysis of Hydroxyl Radicals**

169 The formation of hydroxyl radicals at the photoilluminated photocatalyst/water interface
170 could be detected by a PL technique using terephthalic acid as a probe molecule.[5]
171 Terephthalic acid readily reacted with hydroxyl radicals to produce highly fluorescent
172 product, 2-hydroxyterephthalic acid. The intensity of the PL signal at 425 nm of
173 2-hydroxyterephtalic acid was in proportion to the amount of hydroxyl radicals. PL spectra of
174 the generated 2-hydroxyterephthalic acid were measured on a Hitachi F-4500 fluorescence
175 spectrophotometer. After light irradiation every 20 min, the reaction solution was filtrated to
176 measure the increase of the PL intensity at 425 nm excited by 315 nm light.

177 **Preparation of E. coli for ESEM**

178 E. coli without or with PEC treatment were collected by centrifugation. The pellet was
179 fixed in 2.5% glutaraldehyde for approximately 60 min at room temperature, and then soaked
180 in cacodylate buffer for 10 min to remove excess fixative and post-fixed for 20 min in 1%
181 osmium tetraoxide. Subsequently, the samples were dehydrated by successive soakings in
182 37%, 95% and 100% ethanol each for 10 min, respectively. Critical point drying was

183 performed by placing samples in hexamethyldisilazane for 45 min and overnight drying
184 under a fume hood after drawing the hexamethyldisilazane off. The morphologies of the
185 samples were visualized using an environmental scanning electron microscope.

186 **Preparation of E. coli for TEM**

187 At given time intervals, the cell suspension was collected and centrifuged down to pellets.
188 The bacteria pellets were pre-fixed in 2.5% glutaraldehyde at 4 °C for 12 h and then washed
189 twice with 0.1 M phosphate buffer (PBS) (PH = 7.2). After being washed with PBS, the
190 specimens were mixed with 2% $Na_2H_5[P(W_2O_7)_6]$ aqueous solution with a volume ratio 1:1
191 for 2 h. Then, the mixed suspension was dropped onto the cupper grids with holey carbon
192 film for TEM observation.

193 **TEM and HRTEM Analysis**

194 The microscopic morphology and structural information of Ag/AgBr/TiO_2-NA is
195 investigated by TEM. Figure S2b is a TEM image of the TiO_2 nanotubes, showing that the
196 pure TiO_2-NA has an ordered array tubular structure. The TEM image of Ag/AgBr/TiO_2-NA
197 clearly displays that Ag/AgBr nanoparticles have been deposited on the inner and outer wall
198 of the TiO_2 nanotube (Figure S2c). Further study by HRTEM (Figure S2d-S2e) shows that
199 lattice fringes measured at the interface between Ag/AgBr nanoparticles and TiO_2 nanotubes
200 are finger prints of the crystallographic planes of metallic Ag (111) and (200), cubic AgBr
201 (200) and anatase TiO_2 (101) with lattice spacing of 0.236 nm and 0.204 nm (JCPDS
202 01-1164), 0.288 nm (JCPDS 79-0149) and 0.351 nm (JCPDS 71-1167), respectively. These
203 results confirm that Ag nanoparticles really exist on the surface of the AgBr nanoparticles and
204 the obtained Ag/AgBr nanoparticles have been successfully assembled into TiO_2-NTA.

205 Moreover, HRTEM image of Ag/AgBr/TiO_2-NA shows the existence of coherent interface
206 between the lattice fringes of the Ag, AgBr and TiO_2, indicating that a hetero/nano-junction
207 might be formed, which benefits better separation of photoinduced charge carriers and more
208 efficient electron transfer within the composite structure.

209 **PL Analysis**

210 Figure S3 shows a comparison of the PL spectra of the TiO_2-NA, Ag/TiO_2-NA and
211 Ag/AgBr/TiO_2-NA. A decrease in the photoluminescence intensity of Ag/TiO_2-NA is
212 observed compared with that of pure TiO_2-NA, indicating that the Ag nanoparticles on the
213 TiO_2-NA could reduce the recombination of electron-hole pairs. For the Ag/AgBr/TiO_2-NA,
214 drastic quenching of PL intensity suggests a markedly enhanced charge separation in
215 comparison to the TiO_2-NA, which implies the modification of metallic Ag and AgBr
216 nanoparticles decreases the density of the charge recombination center. Generally, a lower
217 photoluminescence intensity means a lower electron-hole recombination rate, and hence a
218 longer life of the photogenerated carriers.

219 **DRS Analysis**

220 Shown in Figure S4 are UV-Vis DRS spectra obtained from TiO_2-NA, Ag/TiO_2-NA and
221 Ag/AgBr/TiO_2-NA. Pure TiO_2-NA shows an obvious absorption edge below 400 nm and a
222 broad absorption band in the range of 400-700 nm due to the intrinsic band-gap absorption of
223 anatase TiO_2 and the absorption of incident light by nanotube arrays,[6] respectively. In contrast,
224 the absorption edge shifts slightly toward longer wavelength for Ag/TiO_2-NA. Besides, an
225 obvious absorption peak at about 423 nm is also observed as compared to TiO_2-NA in visible
226 light region, which is attributed to the SPR effect of metallic silver.[7] Note that

227 Ag/AgBr/TiO_2-NA has an onset of absorption band significantly red shifted comparing to the
228 TiO_2-NA and Ag/TiO_2-NA. This observation reveals that the deposition of Ag/AgBr
229 nanoparticles can effectively improve the visible-light absorption of the TiO_2-NA, which
230 results from the surface plasmon absorption of metallic Ag and light absorption of AgBr.

231 **Photoelectrochemical Behavior**

232 Figure S5 shows the short-circuit photocurrent time dependence of TiO_2-NA, Ag/TiO_2-NA
233 and Ag/AgBr/TiO_2-NA under visible light irradiation. A considerable rise in the photocurrent
234 responses can be observed for all the samples under visible light irradiation, which is due to
235 the generation and separation of photoinduced electron-hole pairs. The holes are trapped or
236 captured by reduced species in the electrolyte, while the electrons are transported to the Ti
237 substrate via the walls of TiO_2 nanotubes, leading to the effective charge separation. Among
238 the three samples, Ag/AgBr/TiO_2-NA shows a much higher steady state photocurrent density
239 (0.14 mA cm^{-2}) than Ag/TiO_2-NA (0.11 mA cm^{-2}) and TiO_2-NA (0.4 mA cm^{-2}) upon visible
240 light excitation. This result coincides with the UV-Vis DRS and PL spectra perfectly,
241 suggesting that the increase of the photocurrent density is attributed to the enhancement of
242 the visible light adsorption of the Ag/AgBr/TiO_2-NA and improvement of the separation
243 efficiency of photogenerated electron-hole pairs. The minimized electron-hole recombination
244 in this system is due to the contribution of metal Ag and AgBr nanoparticles.

245 **Inactivation Effect of Ag^+ Leakage**

246 Figure 2b shows the inactivation effect of Ag^+ leakage from the Ag/AgBr/TiO_2-NA
247 electrode. It is generally accepted that Ag^+ at high concentrations exhibits bactericidal
248 activity.[8] However, in this work, only a little amount of Ag^+, about 0.27 mg L^{-1} Ag^+, was

249 eluted from Ag/AgBr/TiO_2-NA electrode when it was immerged in suspension of the E. coli.
250 And there was no more Ag^+ leakage even after 2 h of PEC reaction. Moreover, no obvious
251 bactericidal effect was observed in the presence of 0.3 mg L^{-1} Ag^+ even after 2 h. These facts
252 suggest that the inactivation of E. coli should result from the PEC performance of
253 Ag/AgBr/TiO_2-NA electrode instead of the eluted Ag^+.

254 **Monitoring of Intermediates for PEC inactivation of E. coli**

255 The decrease of TOC in the PEC inactivation of E. coli process using the
256 Ag/AgBr/TiO_2-NA electrode was observed and the results were shown in Figure S10. The
257 results showed that the rate of TOC reduction was remarkably slower than that of E. coli
258 (Inset of Figure S10). A 27.2% decrease in TOC was observed after 80 min irradiation while
259 E. coli was almost completely killed, suggesting about quarter biological carbon contents in a
260 cell were completely mineralized and converted into CO_2. The decomposition products of the
261 incomplete-mineralized components are highly complex.

262 In order to better understand the relationship between intermediates generation and
263 damages of the E. coli components, we monitored carboxylic acids (Figure 5c, FTIR Analysis)
264 as the typical intermediates released during E. coli inactivation. As shown in Figure S11,
265 oxamic and oxalic acids are the two main carboxylic acids detected from the PEC
266 inactivation of E. coli process,[9] which arises from the damages to the outer cell membrane
267 proteins and the peroxidation of the phospholipids of the outer cell membrane. Clearly, the
268 concentration of oxamic acids gradually increased in parallel with irradiation time, exhibited
269 a maximum concentration around 320 min, and then further quickly declined. Meanwhile,
270 oxalic acids reached its maximum concentrations at 240 min in the composite electrode

system and then it started to decrease with increasing irradiation time. The results demonstrated that the cell membrane of E. coli was first destroyed by the reactive active species generated from the system, to yield various products including oxamic and oxalic acids. Continuously, these products were further oxidized and degraded by reactive species into the CO_2 and H_2O. Similar to other organic compounds, E. coli required an irradiation time for total mineralization longer than that for the inactivation. Importantly, the intermediates generation has almost no effect on inactivation of E. coli because finally they were also completely mineralized and converted into H_2O and CO_2.

Effect of DBPs on PEC inactivation of E. coli

As we known, traditional water disinfection methods such as chlorination and ozonation have shown disadvantages related to the formation of potentially hazardous DBPs with carcinogenic and mutagenic potential. To find out the influence of the DBPs presence on bactericidal activity during PEC inactivation of E. coli with Ag/AgBr/TiO_2-NA electrode, the series of bacteria inactivation experiments with DBPs like dihydroxybenzene (hydroquinone, resorcinol and catechol) were performed. As shown in Figure S12, the E. coli inactivation rate was obviously decreased with the addition of dihydroxybenzene. The E. coli was completely killed after 91 min irradiation in the presence of resorcinol, and the inactivation rate of E. coli became more slowly with the addition of hydroquinone than with the addition of catechol, resulting in a lower inactivation rate in the presence of hydroquinone (134 min) than in the presence of catechol (120 min). The addition of dihydroxybenzene influences the E. coli inactivation according to the following sequence: hydroquinone > catechol > resorcinol. This order was mainly attributed to the degree of adsorption of different

293 dihydroxybenzene isomers on the Ag/AgBr/TiO_2-NA electrode.[10] Moreover, the time of PEC
294 inactivation of E. coli with Ag/AgBr/TiO_2-NA electrode was longer when the
295 dihydroxybenzenes are present, than without it. This could be explained by the double
296 competition of E. coli and DBPs (dihydroxybenzenes) for oxidation sites on the composite
297 electrode. Firstly, dihydroxybenzenes competed with Ag/AgBr/TiO_2-NA regarding light
298 absorption and then limited the E. coli adsorption on Ag/AgBr/TiO_2-NA. Secondly,
299 photoelectrocatalysis simultaneously deactivated bacteria and degraded dihydroxybenzenes.
300 The latter compounds protected E. coli from PEC inactivation reaction, leading to the
301 decreased E. coli inactivation rate.

302 Figure S13 shows the PEC degradation of dihydroxybenzenes in presence of E. coli under
303 visible light irradiation. The degradation rate order of the dihydroxybenzenes was similar to E.
304 coli inactivation. After 80 min irradiation, 4.24% of hydroquinone, 10.2% of catechol and
305 16.7% of resorcinol were degraded, respectively, indicating that the complete degradation of
306 dihydroxybenzenes needs more irradiation time.

307 Therefore, compared to the traditional water disinfection methods, photoelectrocatalysis
308 technology for inactivation of E. coli did not product the DBPs with carcinogenic and
309 mutagenic, which was in accordance with the FTIR measurements. Even if there were few
310 DBPs produced in PEC inactivation of E. coli process, the effect of the inactivation
311 performance of E. coli was is very small because the generated DBPs would be completely
312 mineralized and converted into H_2O and CO_2.

313 **PEC Inactivation of E. coli under Simulated Sunlight Irradiation**

314 Figure S15 displays the inactivation of E. coli as a function of reaction times on the

315 Ag/AgBr/TiO_2-NA electrode in the direct photolysis, electrochemical process, photocatalysis
316 and photoelectrocatalysis under simulated sunlight irradiation. After 30 min, almost no E. coli
317 can be directly killed by only applying the electrolysis under 0.6 V bias; and direct photolysis
318 reaction only resulted in an inactivation ratio of 23.4%. Compared to direct photolysis, the
319 Ag/AgBr/TiO_2-NA electrode (without bias supply) destroyed 56.5% of the E. coli in the same
320 time. Notably, the photoelectrocatalysis process obtained the fastest inactivation rate and
321 complete inactivation of E. coli was achieved in only 17 min with the bias potential of 0.6 V.
322 Such enhancement confirmed that the bias potential applied in the photoelectrocatalysis
323 process could efficiently separate the photogenerated electron-hole pairs by transporting the
324 photogenerated electron to the counter electrode and therefore inhibiting the recombination.
325 Additionally, the results could also be seen from the representative photographs of the E. coli
326 colonies (Figure S16 and Figure S17). Corresponding TEM and FTIR results (Figure S18 and
327 Figure S19) are similar to that of previous study about photoelectrocatalytic inactivation of E.
328 coli on the Ag/AgBr/TiO_2-NA electrode under visible light irradiation.

329 Figure S20 shows PEC inactivation of E. coli with different catalysts under simulated
330 sunlight irradiation. TiO_2-NA electrode exhibited excellent PEC activity under simulated
331 sunlight irradiation for the inactivation of E. coli and 3.71 logs of E. coli was inactivated after
332 40 min of reaction time. Furthermore, N/TiO_2-NA electrode displayed better PEC activity
333 than TiO_2-NA electrode. After 33 min irradiation, 100% of E. coli was removed, which was
334 48.2% higher than that on TiO_2-NA electrode. When Ag/AgBr/TiO_2 electrode was used as the
335 photocatalyst, the PEC inactivation efficiency of E. coli reached 100% after 37 min simulated
336 sunlight irradiation. While in the case of apatite-covered Ag/AgBr/TiO_2 electrode, the E. coli

was almost completely killed within 26 min under light irradiation. Surprisingly, Ag/AgBr/TiO_2-NA electrode could inactivate 100% of E. coli only within 17 min under the same experiment conditions, indicating the highest PEC antibacterial activity. However, only about 30.1% of E. coli was inactivated over porous TiO_2 electrode (Baram) after irradiation for 40 min. Based on the above results, the PEC antibacterial activity under simulated sunlight irradiation increased in the order of porous TiO_2 < TiO_2-NA < Ag/AgBr/TiO_2 < N/TiO_2-NA < apatite-covered Ag/AgBr/TiO_2 < Ag/AgBr/TiO_2-NA. This result clearly indicated that the composite nanotube structure facilitated the separation of electron and hole pairs, reduced the chance of the recombination and enhanced the efficiency of the light absorption.

As shown in Figure S21, the Ag/AgBr/TiO_2-NA electrode displayed highly efficient antibacterial activity under simulated sunlight irradiation (150 mW cm^{-2}). About 83.1% percentage of the E. coli was inactivated under simulated sunlight irradiation for only 2 min, and all the E. coli was killed within 4 min, which is only a little inferior to the TiO_2 nanotube/CdS electrode under similar experiment conditions.[11] The TiO_2 nanotube/CdS electrode resulted in the PEC inactivation of the E. coli in only 3 min under a white light irradiation (150 mW cm^{-2}). However, in most cases, the stability of the CdS-based photocatalysts is not satisfactory due to the disadvantage of photocorrosion,[12,13] which hinders its practical application. On contrast, the stability in structure and property ensures that Ag/AgBr/TiO_2-NA electrode could be used as an efficient and stable visible-light-driven photocatalyst.

REFERENCES

(1) Lai, Y. K.; Huang, J. Y.; Zhang, H. F.; Subramaniam, V. P.; Tang, Y. X.; Gong, D. G.; Sundar, L.; Sun, L.; Chen, Z.; Lin, C. J. Nitrogen-doped TiO_2 nanotube array films with enhanced photocatalytic activity under various light sources. *J. Hazard. Mater.* **2010,** *184* (1-3), 855-863.

(2) Baram, N.; Starosvetsky, D.; Starosvetsky, J.; Epshtein, M.; Armon, R.; Ein-Eli, Y. Enhanced photo-efficiency of immobilized TiO_2 catalyst via intense anodic bias. *Electrochem. Commun.* **2007**, *9* (7), 1684-1688.

(3) Hu, C.; Lan, Y. Q.; Qu, J. H.; Hu, X. X.; Wang, A. M. Ag/AgBr/TiO_2 visible light photocatalyst for destruction of azodyes and bacteria. *J. Phys. Chem. B* **2006**, *110* (9), 4066-4072.

(4) Elahifard, M. R.; Rahimnejad, S.; Haghighi, S.; Gholami, M. R. Apatite-coated Ag/AgBr/TiO_2 visible-light photocatalyst for destruction of bacteria. *J. Am. Chem. Soc.* **2007**, *129* (31), 9552-9553.

(5) Ishibashi, K.; Fujishima, A.; Watanabe, T.; Hashimoto, K. Detection of active oxidative species in TiO_2 photocatalysis using the fluorescence technique. *Electrochem. Commun.* **2000,** *2* (3), 207-210.

(6) Zhuang, H. F.; Lin, C. J.; Lai, Y. K.; Sun, L.; Li, J. Some critical structure factors of titanium oxide nanotube array in its photocatalytic activity. *Environ. Sci. Technol.* **2007**, *41*, 4735-4740.

(7) Zhang, H. J.; Li, X. Y.; Chen, G. H. Ionic liquid-facilitated synthesis and catalytic activity of highly dispersed Ag nanoclusters supported on TiO_2. *J. Mater. Chem.* **2009,** *19* (43), 8223-8231.

(8) Pal, S.; Tak, Y. K.; Song, J. M. Does the antibacterial activity of silver nanoparticles depend on the shape of the nanoparticle? A study of the gram-negative bacterium Escherichia coli. *Appl. Environ. Microbiol.* **2007,** *73* (6), 1712-1720.

(9) Elsellami, L.; Vocanson, F.; Dappozze, F.; Baudot, R.; Febvay, G.; Rey, M.; Houas, A.; Guillard, C. Kinetics and initial photocatalytic pathway of tryptophan, important constituent of microorganisms. *Appl. Catal. B: Environ.* **2010**, *94* (1-2), 192-199.

(10) Rincón, A. G.; Pulgarin, C. Effect of pH, inorganic ions, organic matter and H_2O_2 on E. coli K12 photocatalytic inactivation by TiO_2 Implications in solar water disinfection. *Appl. Catal. B: Environ.* **2004**, *51* (4), 283-302.

(11) Hayden, S. C.; Allam, N. K.; El-Sayed, M. A. TiO_2 nanotube/CdS hybrid electrodes: extraordinary enhancement in the inactivation of Escherichia coli. *J. Am. Chem. Soc.* **2010**, *132* (41), 14406-14408.

(12) Walter, M. G.; Warren, E. L.; McKone, J. R.; Boettcher, S. W.; Mi, Q. X.; Santori, E. A.; Lewis, N. S. Solar water splitting cells. *Chem. Rev.* **2010**, *110* (11), 6446-6473.

(13) Chen, X. B.; Shen, S. H.; Guo, L. J.; Mao, S. S. Semiconductor-based photocatalytic hydrogen generation. *Chem. Rev.* **2010**, *110* (11), 6503-6570.

397 Figure S1

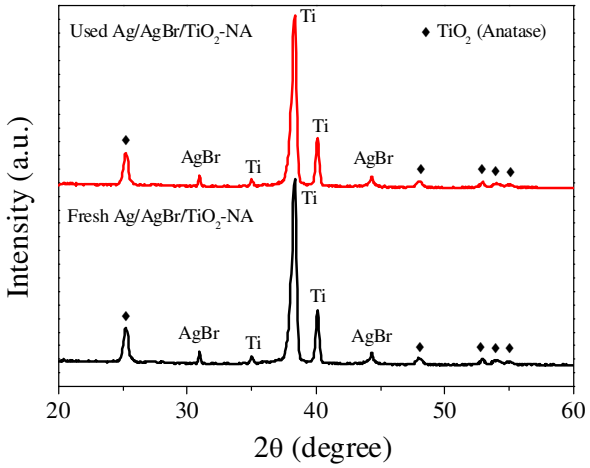

398

Figure S2

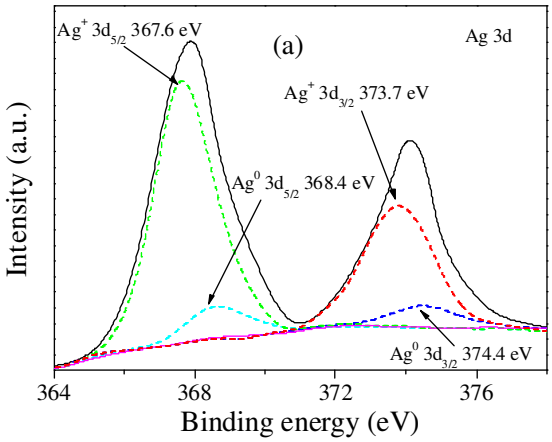
(a)
Ag 3d
Ag+ 3d5/2 367.6 eV
Ag+ 3d3/2 373.7 eV
Ag0 3d5/2 368.4 eV
Ag0 3d3/2 374.4 eV
Intensity (a.u.)
364
368
372
376
Binding energy (eV)

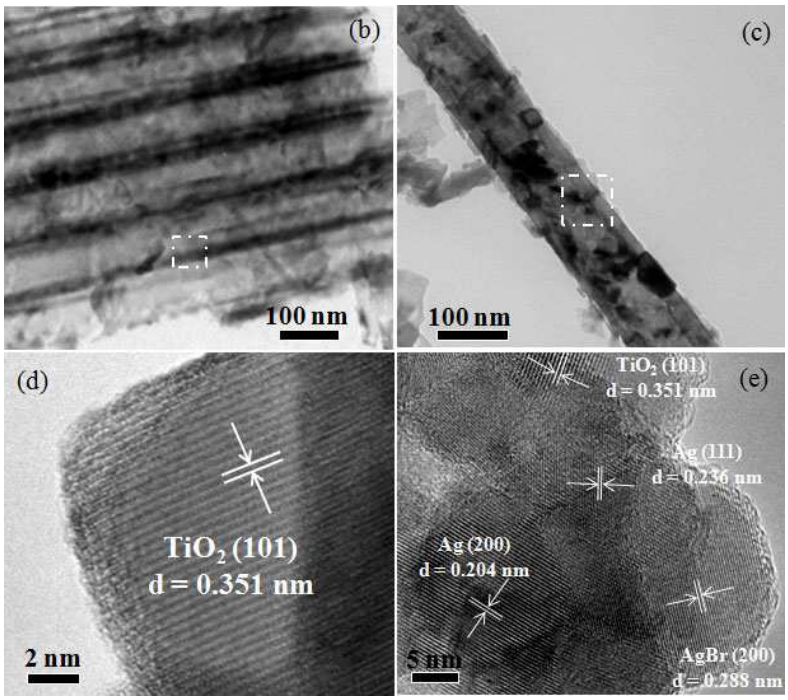
(b)
100 nm
(c)
100 nm
(d)
TiO2 (101)
d = 0.351 nm
2 nm
(e)
TiO2 (101)
d = 0.351 nm
Ag (111)
d = 0.236 nm
Ag (200)
d = 0.204 nm
5 nm
AgBr (200)
d = 0.288 nm

402 Figure S3

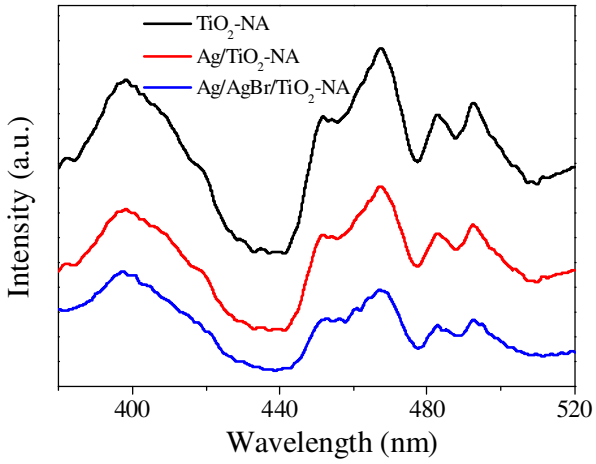

403

404 Figure S4

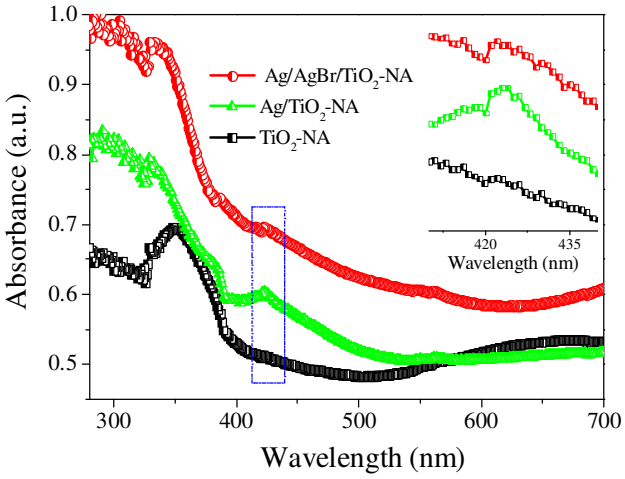

405

Figure S5

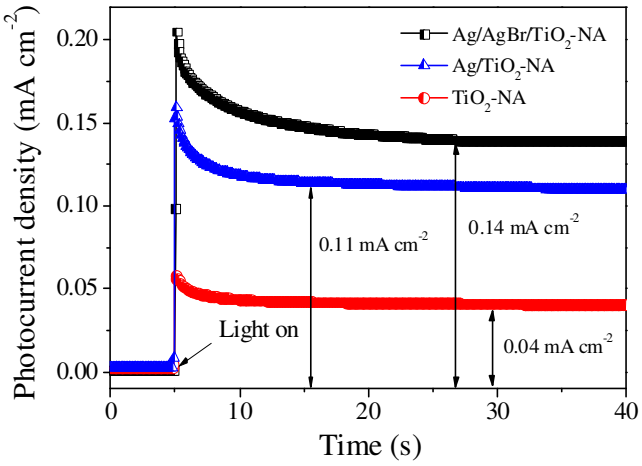
Photocurrent density (mA cm^{-2})
0.20
0.15
0.10
0.05
0.00
0
10
20
30
40
Time (s)
Ag/AgBr/TiO$_2$-NA
Ag/TiO$_2$-NA
TiO$_2$-NA
0.11 mA cm^{-2}
0.14 mA cm^{-2}
0.04 mA cm^{-2}
Light on

408 Figure S6

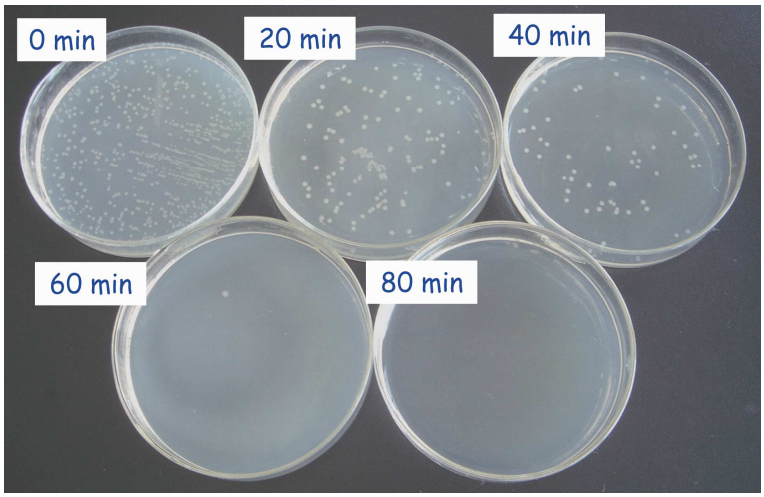

409

Figure S7

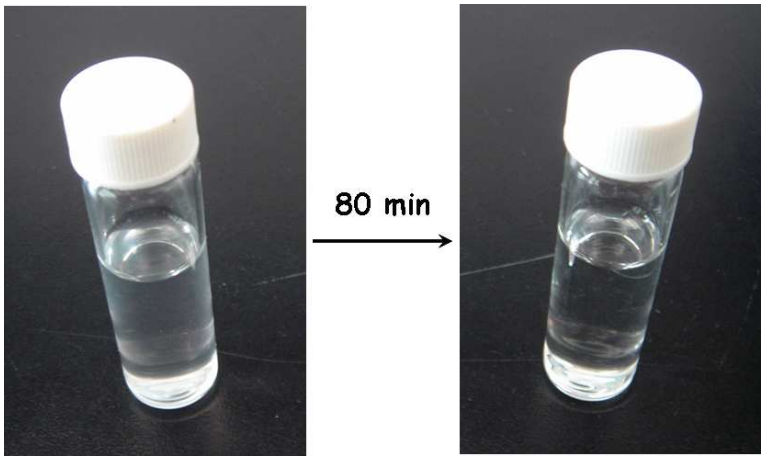

412 Figure S8

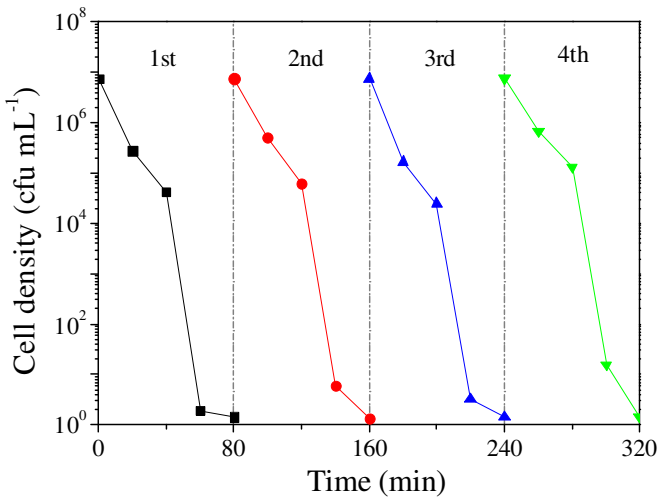

413

Figure S9

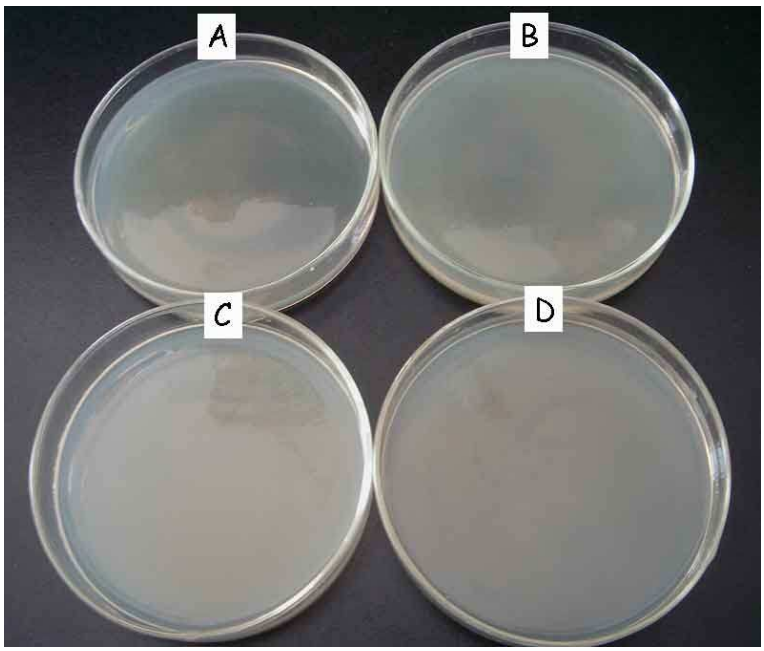

416 Figure S10

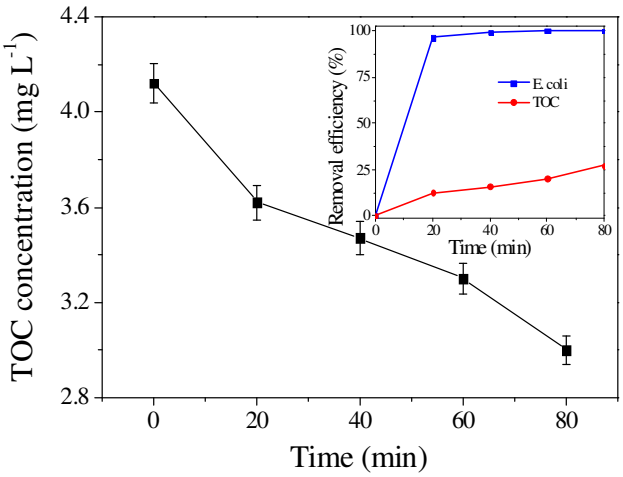

417

418 Figure S11

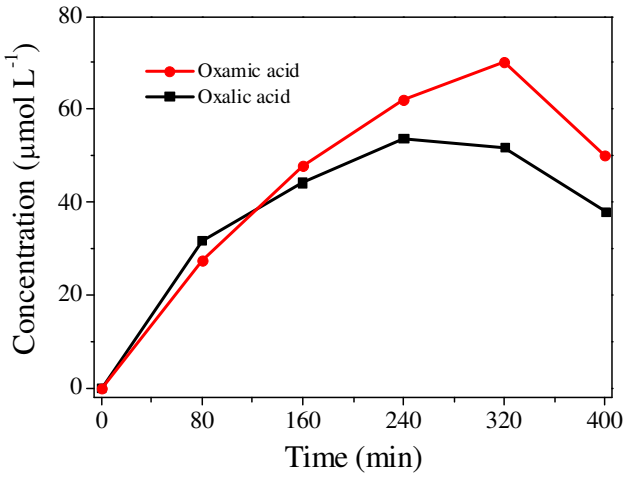

419

420 Figure S12

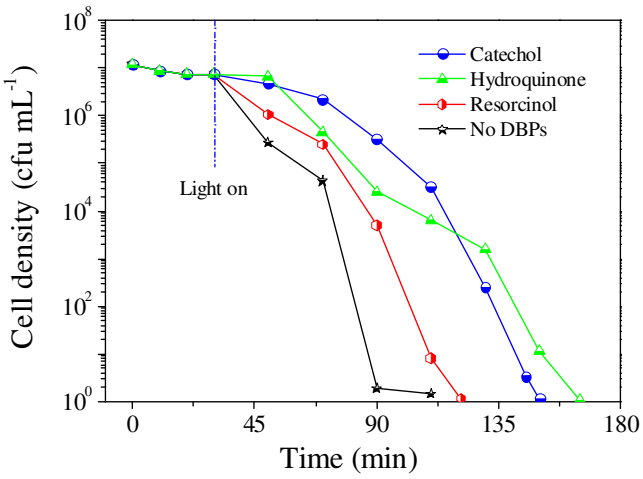

421

422 Figure S13

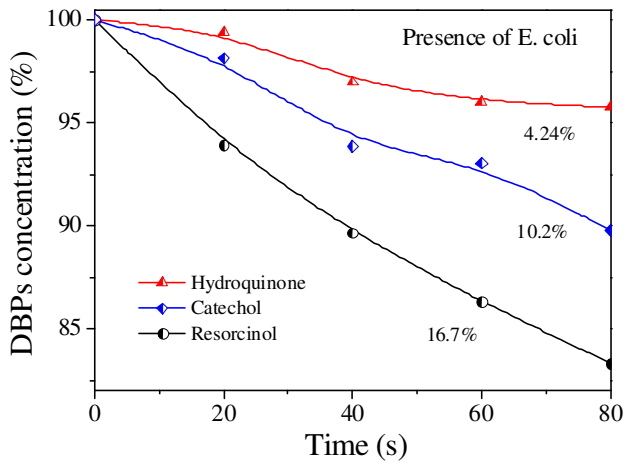

423

Figure S14

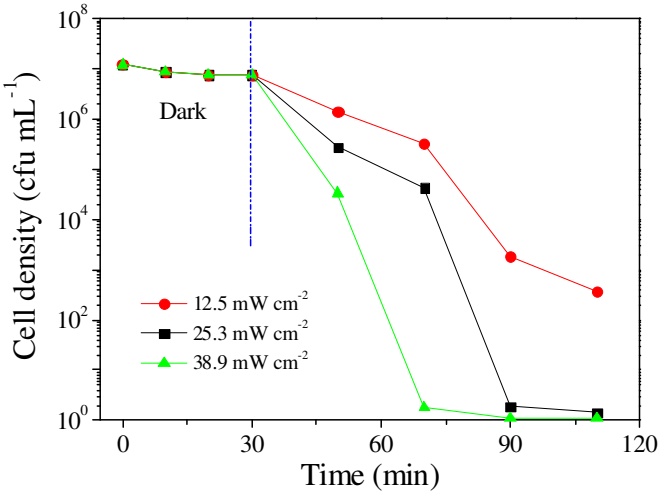
Cell density (cfu mL^{-1})
10^8
10^6
10^4
10^2
10^0
Dark
12.5 mW cm^{-2}
25.3 mW cm^{-2}
38.9 mW cm^{-2}
0
30
60
90
120
Time (min)

426 Figure S15

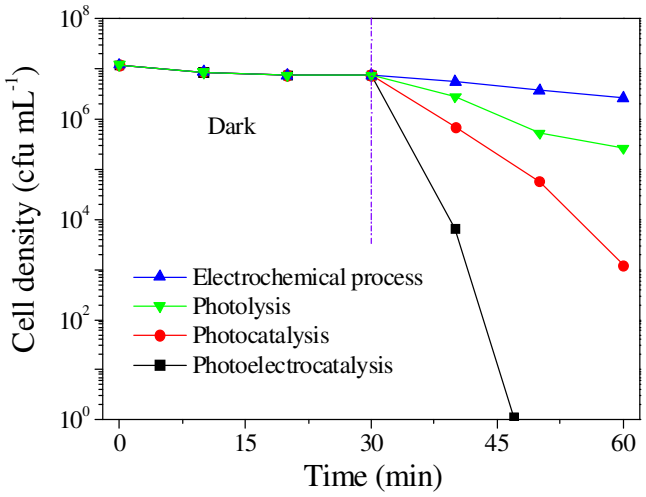

427

428 Figure S16

429 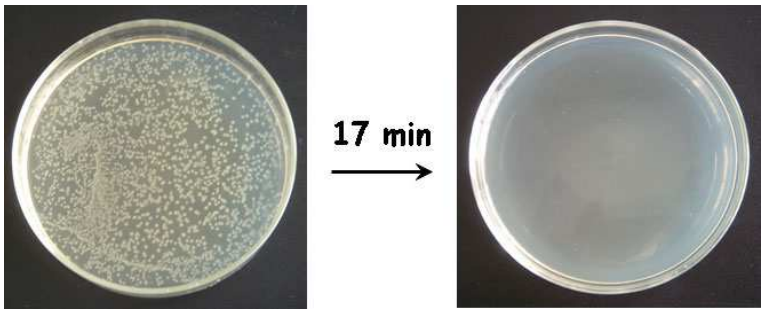

Figure S17

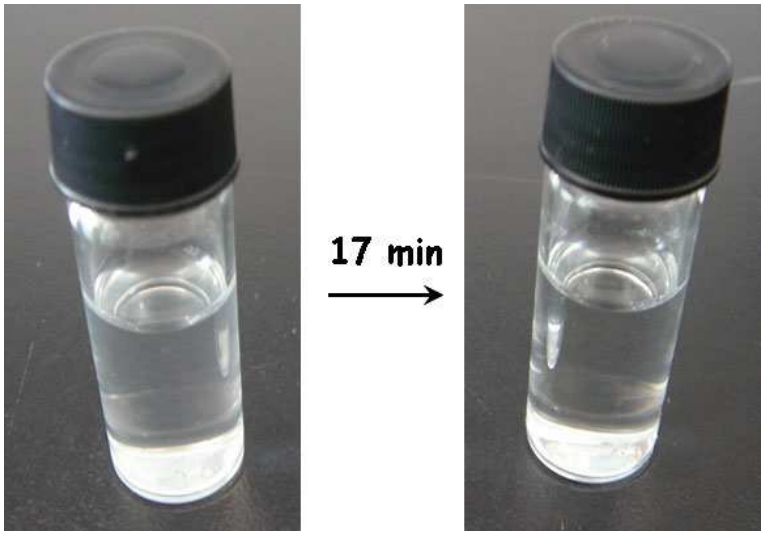

Figure S18

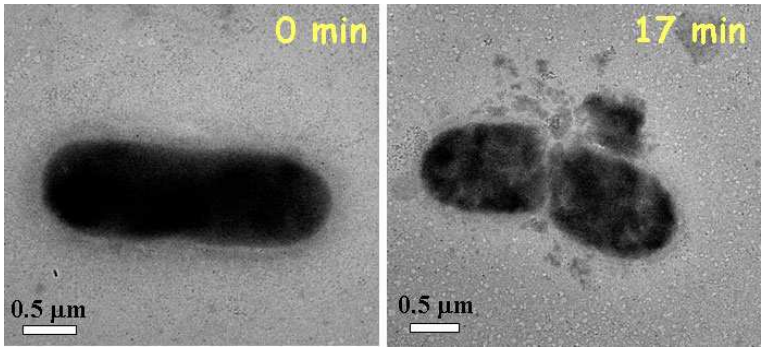

Figure S19

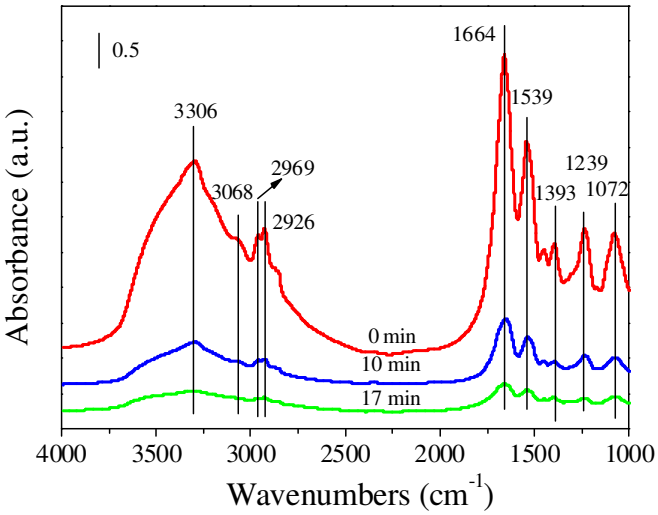
0.5
3306
3068
2969
2926
1664
1539
1393
1239
1072
0 min
10 min
17 min
Absorbance (a.u.)
4000
3500
3000
2500
2000
1500
1000
Wavenumbers (cm-1)

436 Figure S20

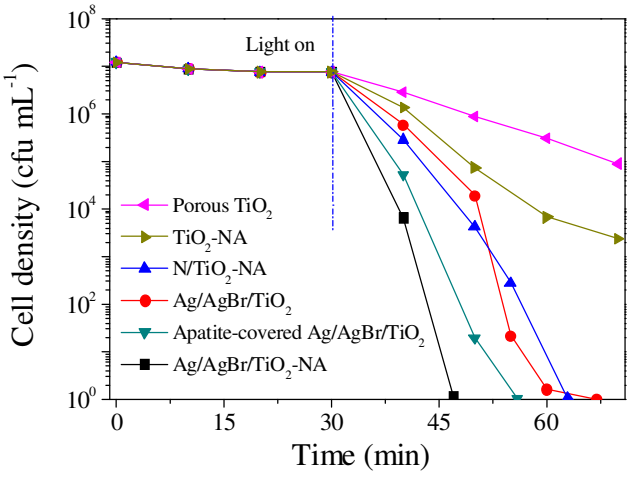

437

438 Figure S21

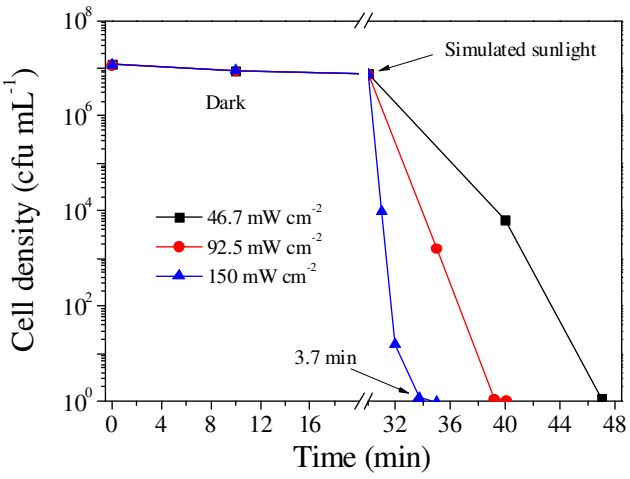

439

Scheme S1

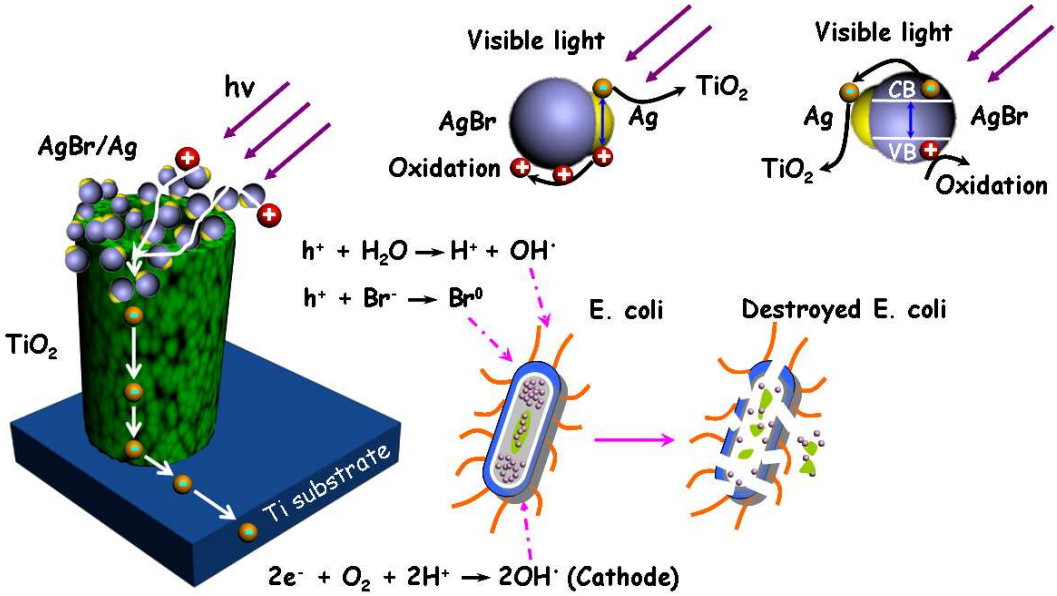
hv
AgBr/Ag
TiO2
Ti substrate
Visible light
AgBr
Ag
TiO2
Oxidation
Visible light
CB
VB
Ag
AgBr
TiO2
Oxidation
h+ + H2O → H+ + OH·
h+ + Br- → Br0
E. coli
Destroyed E. coli
2e- + O2 + 2H+ → 2OH· (Cathode)

Table S1

Frequency (cm^{-1})	Assignment
3297	amide A
3066	amide B
2960	$\nu_a(CH_3)$
2923	$\nu_a(CH_2)$
2870	$\nu_s(CH_3)$
2851	$\nu_s(CH_2)$
1730	aliphatic aldehydes (R-CHO)
1656	amide I
1543	amide II
1400	$\nu_s(O{=}C{-}O^-)$
1334	Carboxylic groups
1237	$\nu_{as}(PO_2^-)$
1083	$\nu_s(PO_2^-)$